Surface Diffusion and Adsorption of Hydrocarbons in Activated Carbon

H. D. Do, D. D. Do, and I. Prasetyo
Dept. of Chemical Engineering, University of Queensland, St. Lucia, Qld 4072, Australia

Adsorption and diffusion in a porous media were studied theoretically and experimentally with a differential transient permeation method. The porous medium is allowed to equilibrate at some specified loading, and then the time trajectory of the permeation process is followed after a small difference between the pressures at the end faces of the porous medium is introduced at time $t = 0+$. Such a trajectory vs. time would contain adsorption and diffusion characteristics of the system. By studying this for various surface loadings, pore and surface diffusions can be fully characterized. Mathematical modeling of transient permeation is detailed for pure gases or vapors diffusion and adsorption in porous media. Effects of nonlinearity of adsorption isotherm, pressure, temperature and heat effects were considered in the model. Experimental data of diffusion and adsorption of propane, n-butane and n-hexane in activated carbon at different temperatures and loadings show the potential of this method as a useful tool to study adsorption kinetics in porous media. Validity of the model is best tested against the transient data where the kinetics curves exhibit sigmoidal shape, which is a result of the diffusion and adsorption rate during the initial stage of permeation.

Introduction

Adsorption kinetics in complex porous media has been a topic of great interest in adsorption separation and purification. Numerous works have appeared in the literature, and the various aspects of adsorption kinetics have been addressed in various books (Ruthven, 1984; Yang, 1987; Suzuki, 1990; Do, 1997, 1998). Although some aspects have been understood, many are not very well known, for example, the role of pore texture (size and configuration) on the adsorption kinetics, especially the surface diffusion and the mass exchange between the intraparticle fluid phase and the adsorbed phase. To achieve this goal, researchers have used various experimental techniques to measure the adsorption kinetics. Most of these techniques only provide macroscopic information about the kinetics, and therefore a mathematical model must be developed. In addition, many conditions are experimentally covered to validate the model. The goal is to have a model (sufficiently comprehensive) with the least number of fitting parameters, and of course an ultimate goal is to find one in which all parameters could be independently estimated or calculated. At the present state of knowledge, we are still a long way from that ultimate goal. Nevertheless, we are developing a better model as we learn more about our adsorption systems. To achieve this, we need to use a variety of tools, as suggested recently by Bulow and Micke (1995), to fully explore the kinetics behavior of a system.

We present in this article a permeation method operated under steady state and transient modes to study the behavior of an adsorption system. This method has advantages over many other methods, and is easy to carry out experimentally. Differential conditions can be easily maintained with this apparatus, and therefore the heat effect can be kept to a minimum or completely eliminated with careful design. The two aspects that we concentrate on are the medium topology and the surface diffusion. These aspects are taken into account in the model development. Other processes and factors accounted for in the model are Knudsen diffusion, viscous flow, nonlinear adsorption, heat effect, and the various operating conditions.

The permeation method is very easy to set up, with the most delicate step being the mounting of the porous medium between the two reservoirs that are either closed or semiopen. In our work, we mount one activated carbon extrudate in a

Correspondence concerning this article should be addressed to D. D. Do.

Table 1. Constitutive Equations and Temperature-Dependent Parameters

	Constitutive Equation		Temperature-Dependent Transport Coefficient	
Pore diffusion	$N_p = -\frac{D_p(T)}{R_g T}\frac{\partial p}{\partial z}$	(2a)	$D_p = \frac{D_K}{q} = \frac{4K_0}{3q}\sqrt{\frac{8R_g T}{\pi M}}$	(3a)
Viscous flow	$N_v = -\frac{B_0 p}{\mu R_g T}\frac{\partial p}{\partial z}$	(2b)	$\mu = \mu_0\left(\frac{T}{T_0}\right)^{\alpha}$	(3b)
Surface diffusion	$N_\mu = -D_\mu^0(T, C_\mu)\frac{C_\mu}{p}\frac{\partial p}{\partial z}$	(2c)	$D_\mu^0(T, C_\mu) = D_\mu^{00}(T)\exp\left(\frac{E_{\mu 0}}{RT}\frac{\beta C_\mu}{1+BC_\mu}\right)$	
			$D_\mu^{00}(T) = D_{\mu 0}^{00}\exp\left[\frac{E_{\mu 0}}{RT_0}\left(1-\frac{T_o}{T}\right)\right]$	(3c)

predrilled copper block. The hole size of the copper block is just slightly larger than the radius of the extrudate. The extrudate is then placed inside the hole of the copper block, and the annulus gap between the extrudate and the copper block is sealed with high-temperature epoxy so that there are no cracks or channels joining the two reservoirs. The only route for mass flow and diffusion between the two reservoirs is through the porous medium. The activated carbon-/copper-block assembly is then joined to the two reservoirs through conflat fittings.

The experimental procedure is simple, as shown in the following basic steps:

1. Clean the two reservoirs and the porous medium by thorough vacuum pumping and heating
2. Fill the system (two reservoirs and porous medium) with gas or vapor up to some determined pressure and allow the system to achieve equilibrium
3. Isolate the upstream reservoir from the rest
4. Add gas or vapor into the upstream reservoir such that its pressure is increased by a very small amount; then the upstream reservoir is reconnected allowing the differential flow and diffusion to take place.

Various operations could also be carried out, for example, in step 3 the downstream reservoir is isolated instead of the upstream reservoir, or in step 4 the pressure is decreased by a small amount rather than increased. Another feature that can be exploited is that a constant molar flow is introduced into the upstream reservoir. This constant molar flow is chosen experimentally such that its magnitude is comparable to the molar flow rate through the porous medium.

Theory

The system of permeation is simple and straightforward. Here a porous particle is mounted between the two reservoirs. This is done very carefully such that there is no crack or gap between the two reservoirs. The mass transfer from one reservoir to another is through the porous particle. We shall deal with flow and diffusion of pure gases or vapors in this article.

The mathematical model will involve the mass balances in the particle and in the two reservoirs coupled with the heat balance due to the heat released by the rate of adsorption. Typical heat of adsorption of many hydrocarbons, carbon oxides on activated carbon, alumina, or silica materials ranges from 10 kJ/mol to 60 kJ/mol. Such a magnitude can cause a significant change in the particle temperature if the dissipation of energy to the surrounding is not fast enough or the rate of adsorption is relatively fast (for example, in very small particles). Thus, the particle-temperature increase (in adsorption) or decrease (in desorption) depends on the interplay between the rate of heat release due to adsorption and the dissipation rate of energy to the surrounding area. It is important that we address this heat effect and determine whether the heat effect can cause any interference with the mass transfer for systems of hydrocarbons diffusing and adsorbing in activated carbon.

Problem formulation

Mass-Balance equation. The mass-balance equation over the thin shell of a particle in which Knudsen diffusion, viscous flow, and surface diffusion are operative is

$$\epsilon\frac{\partial}{\partial t}\left(\frac{p}{R_g T}\right) + (1-\epsilon)\frac{\partial C_\mu}{\partial t} = -\frac{\partial}{\partial z}\left[\epsilon N_p + \epsilon N_v + (1-\epsilon)N_\mu\right], \quad (1)$$

where p is the intraparticle pressure (Pa); C_μ is the adsorbed phase concentration (mol/m^3 of the solid), which is a function of intraparticle pressure and temperature; ϵ is the porosity of the through-pores; N_p is Knudsen flux (based on empty cross-sectional area) of adsorbate through the void volume; N_v is the viscous flux (based on empty cross-sectional area); and N_μ is the flux of adsorbate in the adsorbed phase. We shall assume that there will be no capillary condensation in the porous medium, and therefore the through-pore porosity ϵ is taken as constant during the whole course of diffusion and adsorption. The effect of capillary condensation will be dealt with in a future publication.

The flux equations for N_p, N_v, and N_μ are assumed to take the form listed in Table 1. Also listed in the table is the temperature dependence of the various transport coefficients. In this table, the parameter q is the tortuosity factor ($= 3$ for isotropic media; Johnson and Stewart, 1965), and K_0 is the Knudsen flow parameter, which is a function of solid charac-

teristics only. The parameter B_0 is the viscous flow parameter, and μ is the fluid viscosity, with μ_0 being the viscosity at some reference temperature T_0.

Equation 2c in the table is the expression for the surface-diffusion flux, derived assuming (1) the driving force for surface diffusion is the gradient of the chemical potential, and (2) the mobility constant is a function of adsorbed concentration, instead of constant, as in the traditional Darken theory. The reason for assumption (2), made in this work, is that our experimental data of many hydrocarbons in activated carbon have shown that the permeability for surface diffusion, $B_\mu = D_\mu^0 \times (C_\mu/p)$, increases with loading. This means that if the corrected diffusivity D_μ^o is taken to be constant, as assumed by Darken, then the surface permeability would decrease with loading, rather than increasing, as observed experimentally. To account for this experimental fact, we have to assume that the activation for surface diffusion follows the following function with the loading:

$$E_\mu = E_{\mu 0}\left(1 - \frac{\beta C_\mu}{1+\beta C_\mu}\right), \tag{4}$$

where the parameter β is a measure of how fast the activation energy for surface diffusion decreases with loading. With this function form for the activation energy for surface diffusion (Eq. 4), the corrected diffusivity is a function of loading, as shown in Eq. 3c. Here the parameter D_μ^{00} is the corrected diffusivity at zero loading, and $D_{\mu o}^{00}$ is the zero-loading corrected diffusivity at the reference temperature, T_0. The parameter $E_{\mu 0}$ is the activation energy for surface diffusion at zero loading. This activation energy has been found experimentally to fall in the range of $Q/3 < E_\mu < Q$ (Carman, 1956; Sladek et al., 1974; Kapoor et al., 1989), where Q is the heat of adsorption.

As seen in Eqs. 2, all the fluxes are expressed in terms of the pressure gradient, and hence the coefficient is the respective permeability. The Knudsen permeability is independent of pressure, and the viscous permeability increases linearly with pressure. The surface permeability increases with loading, and this is due to the increase in the corrected diffusivity $D_\mu^0(T,C_\mu)$, which is more than enough to compensate for the decrease in the partition between the two phases (C_μ/p).

Substituting the constitutive flux equations (Eqs. 2) contained in Table 1 into the mass-balance equation (Eq. 1), we get:

$$\epsilon\frac{\partial}{\partial t}\left(\frac{p}{RT}\right) + (1-\epsilon)\frac{\partial C_\mu}{\partial t} = \frac{\partial}{\partial z}\left\{\left[\frac{\epsilon D_p(T)}{RT} + \frac{\epsilon B_0 p}{\mu RT} + (1-\epsilon)D_\mu^0(T,C_\mu)\frac{C_\mu}{p}\right]\frac{\partial p}{\partial z}\right\}. \tag{5}$$

The term in square brackets on the righthand side (RHS) of Eq. 5 is the differential total permeability, contributed by Knudsen diffusion, viscous flow, and surface diffusion. This differential total permeability can be obtained from steady-state experiments where the differential conditions are maintained, that is, the pressure difference across the particle is kept sufficiently small. This differential total permeability is denoted as $B(p,T)$

$$B(p,T) = \epsilon\frac{D_p(T)}{RT} + \frac{\epsilon B_0 p}{\mu(T)RT} + 1(1-\epsilon)D_\mu^0(T,C_\mu)\frac{C_\mu(p,T)}{p}. \tag{6}$$

For the typical activated-carbon size used in practice (on the order of millimeters) and the time scale of adsorption (on the order of minutes or longer), it is reasonable to assume that the local equilibrium is established between the intraparticle fluid phase and the adsorbed phase:

$$C_\mu = f(p,T). \tag{7}$$

For substances with constricted pores, such as in a carbon molecular sieve, the local equilibrium assumption may not hold (Nguyen and Do, 1999). Do and Wang (1999a,b) have addressed the effect of this finite mass exchange between the two phases on the overall adsorption kinetics, and for particle size greater than about 1 mm, it was found that the local equilibrium assumption is valid.

Since the two phases are in local equilibrium with each other, the adsorption isotherm equation (Eq. 7) can be used to eliminate C_μ from Eq. 5 to obtain a mass-balance equation, describing the variation of the pressure within the particle. The pressures at the two end faces of the particle are denoted as p_{b1} and p_{b2}, and they are described by the following mass-balance equations of the two reservoirs:

$$\frac{d}{dt}\left(\frac{V_1 p_{b1}}{RT_{b1}}\right) = A\left[B(p,T)\frac{\partial p}{\partial z}\right]_{z=0} \tag{8a}$$

$$\frac{d}{dt}\left(\frac{V_2 p_{b2}}{RT_{b2}}\right) = -A\left[B(p,T)\frac{\partial p}{\partial z}\right]_{z=L}, \tag{8b}$$

where V_1 and V_2 are volumes of the upstream and downstream reservoirs, respectively.

Heat-Balance Equation. To solve the mass balance equations (Eqs. 5 and 8), we need to derive the heat-balance equation, which describes the variation of particle temperature with time. Since we have molar flow through the particle in the gaseous phase as well as in the adsorbed phase, the heat-balance equation involves balance between the enthalpy in, the enthalpy out, and the heat generation by the adsorption onto solid interior surfaces. It is this molar flow of adsorbate through the particle that makes the particle temperature vary with distance along the particle as well as time. Taking a thin shell in the particle, we derive the following heat-balance equation describing the temperature change with time

and distance along the particle:

$$\frac{\partial}{\partial t}\left\{\left[\epsilon\rho_G c_{pG}+(1-\epsilon)\rho_\mu c_{p\mu}+(1-\epsilon)\rho_s c_{ps}\right](T-T_b)\right\}$$
$$=(1-\epsilon)Q\frac{\partial C_\mu}{\partial t}+k_{eff}\frac{\partial T^2}{\partial z^2}-MW\frac{\partial}{\partial z}\left\{\left[(\epsilon N_p+\epsilon N_v)c_{pG}+(1-\epsilon)N_\mu c_{p\mu}\right](T-T_b)\right\}-a_H h_f(T-T_b), \quad (9)$$

for $0<z<1$, where $\partial C_\mu/\partial t$ is the rate of adsorption per unit solid volume; the parameter h_f is the heat-transfer coefficient per unit surface area; a_H is the heat-transfer surface area per unit volume; Q is the molar heat of adsorption, T_b is the surrounding temperature; and c_p is specific heat. The gaseous density and the adsorbed phase density are related to the corresponding pressure and concentration as follows:

$$\rho_G=MW\frac{p}{RT};\qquad \rho_\mu=MW\times C_\mu. \quad (10)$$

Here we assume the ideal gas law for the gaseous phase. A more proper equation of state, such as the Peng-Robinson equation, can be used to calculate the gaseous density, but since the vapor pressure is rather low for the substances dealt with in this article, the ideal gas assumption is a reasonable approximation. We take *n*-hexane, for example. At 303 K, the vapor pressure of *n*-hexane, is 2.5×10^4 Pa. The calculated compressibility at a pressure 2×10^4 Pa (close to the vapor pressure) is 0.99, which is very close to unity, justifying the use of the ideal gas equation. For propane at the same temperature and pressure, the calculated compressibility is 0.997, also very close to unity. Thus we will use the ideal gas equation in the simulation to calculate the gaseous density.

The first term on the RHS of Eq. 9 is the heat generation by adsorption per unit volume of the particle, the second term is the net enthalpy in and out of the differential element, and the last term is the heat dissipation to the bulk surrounding.

The heat-balance equations for the heat balance around the two reservoirs are:

$$\frac{d}{dt}\left[\frac{V_1(MW)p_{b1}c_{pG}(T_{b1}-T_b)}{RT_{b1}}\right]=A\,k_{\text{eff}}\left.\frac{\partial T}{\partial z}\right|_{z=0}$$
$$-A(MW)\left[(\epsilon N_p+\epsilon N_v)c_{pG}+(1-\epsilon)N_\mu c_{p\mu}\right]_{z=0}(T_{b1}-T_b)-A_{v1}h_{v1}(T_{b1}-T_b) \quad (11a)$$

$$\frac{d}{dt}\left[\frac{V_2(MW)p_{b2}c_{pG}(T_{b2}-T_b)}{RT_{b2}}\right]=-A\,k_{\text{eff}}\left.\frac{\partial T}{\partial z}\right|_{z=L}$$
$$-A(MW)\left[(\epsilon N_p+\epsilon N_v)c_{pG}+(1-\epsilon)N_\mu c_{p\mu}\right]_{z=L}(T_{b2}-T_b)-A_{v2}h_{v2}(T_{b2}-T_b). \quad (11a)$$

The Boundary and Initial Conditions. The boundary conditions of the mass-balance equation (Eq. 7) are

$$r=0;\qquad p=p_{b1} \quad (11b)$$
$$r=L;\qquad p=p_{b2}. \quad (11b)$$

We assume that the particle is initially equilibrated with a pressure of p_i and a temperature of T_i, that is,

$$t=0;\qquad p=p_i;\qquad C_{\mu,i}=f(p_i,T_i);\qquad T=T_i. \quad (12)$$

The initial temperature T_i may not be the same as the surrounding temperature T_b. Although there is no variation in the initial intraparticle pressure with distance, the nonuniformity of the initial intraparticle pressure ($p_i(r)$) can be dealt with easily in this model.

Numerical solution

The set of governing equations (Eq. 8 to 12) are nonlinear partial differential equations, and they are effectively solved by the combination of the orthogonal collocation method and a standard integration method.

Simulation Results and Discussion

We first discuss the differential total permeability, which is the steady-state molar flux per unit pressure gradient. Its variation with pressure and temperature are discussed for the following two cases: (1) linear isotherm when the pressure is very low, and (2) Langmuir isotherm. In the second case we investigate the effect of the nonlinear curvature of the adsorption isotherm.

Steady-state permeability for linear isotherm

At low pressure, the adsorption isotherm is linear, $C_\mu=K(T)p$, where $K(T)$ is the Henry constant and is only a function of temperature. The differential total permeability (Eq. 6) will take the form:

$$B(p,T)=\frac{16\epsilon K_0}{3q}\frac{1}{\sqrt{2\pi MRT}}+\frac{\epsilon B_0 p}{\mu_0(T/T_0)^\alpha RT}+(1-\epsilon)D_\mu^{00}(T)K(T). \quad (13)$$

If the Henry constant $K(T)$ has the following temperature dependence

$$K(T)=K_\infty\exp(Q/RT), \quad (14)$$

then the permeability will take the form

$$B(p,T)=\frac{16\epsilon K_0}{3}\frac{1}{\sqrt{2\pi MRT}}+(1-\epsilon)D_{\mu\infty}^{00}\exp\left(\frac{Q-E_\mu}{RT}\right). \quad (15)$$

Here we have ignored the viscous flow, as is usually the case for most practical adsorbents at very low pressure. Since the heat of adsorption is greater than the activation energy for surface diffusion, when temperature is increased, both the Knudsen and surface diffusion permeabilities decrease.

As seen in Eq. 15, the permeability is a function of temperature, and it is independent of pressure in the Henry law

region. Thus if any pressure or loading dependence is observed for the total permeability, it must be due to the presence of viscous flow and/or surface diffusion in the nonlinear range of the isotherm. This is discussed next.

Steady-state permeability for nonlinear isotherm

To see the pressure dependence of the permeability, we need to consider the region away from the Henry-law region. Let us illustrate this point by using the following Langmuir equation:

$$C_\mu = f(p,T) = C_{\mu s}\frac{b(T)p}{1+b(T)p}, \tag{16a}$$

where the Henry constant $K(T) = C_{\mu s}b(T)$ and the affinity constant takes the form

$$b = b_\infty \exp\left(\frac{Q}{R_g T}\right) = b_0 \exp\left[\frac{Q}{R_g T_0}\left(\frac{T_0}{T}-1\right)\right]. \tag{16b}$$

With this Langmuir form, the permeability $B(p,T)$ has the following explicit form:

$$B(p,T) = \frac{16\epsilon K_0}{3q}\frac{1}{\sqrt{2\pi MRT}} + \frac{\epsilon B_0 p}{\mu_0 (T/T_0)^\alpha RT} + (1-\epsilon)D^{00}_{\mu\infty} g(C_\mu)\frac{bC_{\mu s}}{(1+bp)}\exp\left(\frac{Q-E_\mu}{RT}\right). \tag{17}$$

We see that the dependence of the total permeability on pressure and temperature is somewhat more complicated than for the case of linear isotherm. Nevertheless, we could derive some useful qualitative information from this equation:

1. The Knudsen diffusion term is independent of pressure and it is inversely proportional to the square root of temperature;
2. The viscous flow permeability increases linearly with pressure and it decreases with temperature stronger than that of Knudsen diffusion;
3. The surface diffusion permeability can either increase or decrease with pressure, depending on the magnitude of the parameters β's (Eq. 4). Experimental data have shown that this surface permeability increases with loading (pressure). The temperature dependence of the surface diffusion term is more complicated due to the interaction between the variation of the intrinsic surface mobility and the adsorbed concentration with temperature.

Table 2. Base Parameters Used in the Simulation

Particle characteristics		
d_p	$= 1.6\times10^{-3}$ m	particle diameter
L	$= 4\times10^{-3}$ m	particle length
ϵ	$= 0.33$	macropore porosity
r_p	$= 8\times10^{-7}$ m	mean macropore radius
ρ_p	$= 717$ kg/m^3	particle density
C_p	$= 750$ J/kg/K	specific heat capacity
k_{eff}	$= 1.1$ J/m/K/s	effective thermal conductivity
q	$= 4.7$	tortuosity factor
Reservoir		
V_1	$= 12.15\times10^{-3}$ m^3	upstream reservoir volume
V_2	$= 38.9\times10^{-6}$ m^3	downstream reservoir volume
a_{V1}	$= 0.2$ m^2	heat-transfer area of the upstream volume
a_{V2}	$= 0.002$ m^2	heat-transfer area of the downstream volume
Reference conditions		
P_0	$= 1$ atm	reference pressure
T_0	$= 303$ K	reference temperature
Adsorbate		
MW	$= 0.058$ kg/mol	molecular weight
μ_0	$= 0.7\times10^{-5}$ kg/m/s	viscosity at reference conditions
c_{pG}	$= 5.3\times10^3$ J/kg/K	specific heat of the adsorbate in gaseous phase
$c_{p\mu}$	$= 5.3\times10^3$ J/kg/K	specific heat of the adsorbate in adsorbed phase
Adsorbate-adsorbent		
b_{10}	$= 0.00723$ Pa^{-1}	adsorption affinity at reference temperature for patch 1
b_{20}	$= 0.0002184$ Pa^{-1}	adsorption affinity at reference temperature for patch 2
$C_{\mu s1}$	$= 2.333\times10^3$ mol/m^3	saturation capacity for patch 1
$C_{\mu s2}$	$= 4.066\times10^3$ mol/m^3	saturation capacity for patch 2
Q_1	$= 44227$ J/mol	heat of adsorption for patch 1
Q_2	$= 45123$ J/mol	heat of adsorption for patch 2
$D^{00}_{\mu 0}$	$= 2.\times10^{-10}$ m^2/s	surface diffusivity at zero laoding and at reference T_0
β	$= 2.8\times10^{-4}$ m^3/mol	the parameter in Eq. 4
$E_{\mu 0}$	$= 15{,}000$ J/mol	activation for surface diffusion at zero loading
Other paratmeters		
h_f	$= 25$ J/m^2/s/K	heat-transfer coefficient from the particle to surrounding
h_{v1}	$= 25$ J/m^2/s/K	HTC from upstream reservoir to surrounding
h_{v2}	$= 25$ J/m^2/s/K	HTC from downstream reservoir to surrounding

Thus the pressure dependence can be utilized to delineate the viscous flow and the surface diffusion from the Knudsen diffusion.

Sensitivity study

Before testing the preceding model with the experimental data, we test the sensitivity of the pressure response in terms of the various parameters of the system. We do this to determine what parameters are the ones that affect most the permeation rate of pure gases and vapors through a porous activated carbon. In our permeation experiments, the upstream reservoir is very large compared to the downstream reservoir. Its large volume is such that when the upstream pressure is increased by a small quantity, and the permeation process is started, the loss of mass from the upstream reservoir due to an increased adsorption in the particle and an increase in the downstream reservoir is so small that the upstream pressure is practically constant. This is done purely for the convenience of experiments. The model, however, can deal with the general case when the upstream pressure varies due to the loss of mass to the particle and the downstream reservoir.

For the purpose of sensitivity study, for the system we choose the parameters of *n*-butane/activated carbon. Those parameters are listed in Table 2. The adsorption isotherm parameters were obtained from the fitting of the dual Langmuir isotherm against the experimental data (more about this will be discussed later in the subsection on testing with the experimental data of propane, *n*-butane, and *n*-hexane).

$$C_\mu = C_{\mu s,1}\frac{b_1 P}{1-b_1 P} + C_{\mu s,2}\frac{b_2 P}{1+b_2 P}. \qquad (18)$$

Effect of Surface Diffusivity. One of the main purposes of this permeation method is to study the surface diffusion and to derive information about it. Therefore the sensitivity of the pressure response vs. time with surface diffusivity is important for evaluating this method as a potential tool to study surface diffusion. Figure 1 shows the sensitivity of the downstream pressure rise vs. time with the variation of the surface diffusivity. Curves *A*, *B*, and *C* correspond to different values of the corrected surface diffusivity at zero loading, with *A*, *B*, and *C* corresponding to 2×10^{-9}, 2×10^{-10} cm^2/s, and 0 cm^2/s. The value of 2×10^{-10} cm^2/s is the surface diffusivity of *n*-butane at 30°C (curve *B*). Here we observe that the sensitivity of the pressure response curve with the variation of the surface diffusivity is very strong good for studying the surface diffusion of hydrocarbons in activated carbon. This is due to the significant contribution of the surface-diffusion flux toward the total mass transfer through the particle. Had the surface diffusion not been significant, curves *A*, *B*, and *C* would have been very close to each other. A similar observation about the sensitivity is also observed for propane and *n*-hexane.

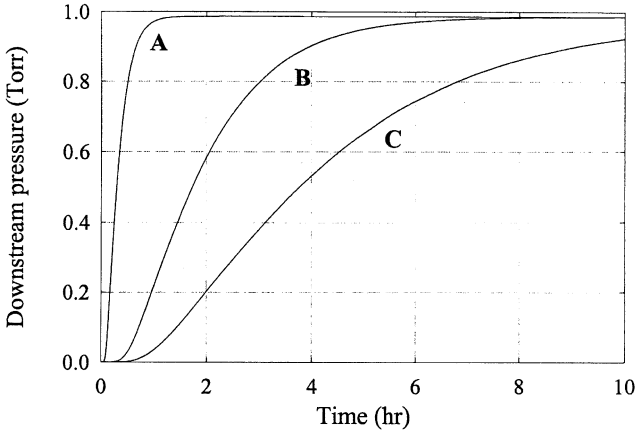

Figure 1. Effect of surface diffusivity on downstream-pressure response vs. time, system: *n*-butane carbon.

$A = 2\times10^{-9}$ cm^2/s, $B = 2\times10^{-10}$ cm^2/s, $C = 0$.

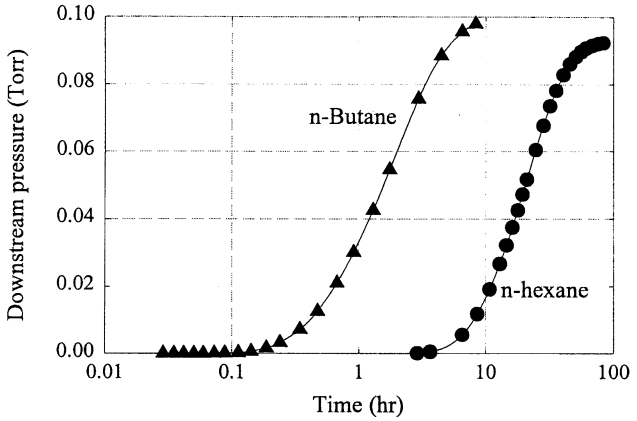

Figure 2. Pressure response of downstream reservoir vs. time for *n*-butane and *n*-hexane

Effect of Adsorbate of Different Affinity. The effect of different adsorbates diffusing and flowing through a particle 4 mm long is shown in Figure 2 for *n*-butane and *n*-hexane. The temperature is 303 K, and the upstream pressure is maintained at 0.1 torr. This figure shows the downstream pressure rise vs. time, and that the sorbate with the stronger affinity will exit the particle later than the weaker adsorbing species. The fitting of transient curves is ideal for extracting the kinetics parameters, in this case, the surface-corrected diffusivity at zero loading. We note that these curves show a sigmoidal shape during the early stage of mass transfer. This is the result of the adsorption onto the solid surface, which then retards the penetration of the concentration wavefront into the downstream reservoir. For strongly adsorbing vapor, *n*-hexane, the time taken for diffusing through the particle is on the order of 2 h, while for the weaker adsorbing gas, *n*-butane, this penetration time is only 0.1 h. The time scale in Figure 2 is in log scale to highlight the time scales of penetration of the two adsorbates.

Effect of Particle Length. The effect of length is shown in Figure 3 for two particle lengths: 4 and 6 mm. The longer particle will provide greater resistance to flow, and hence the breakthrough time is greater in the longer cell, as one would expect.

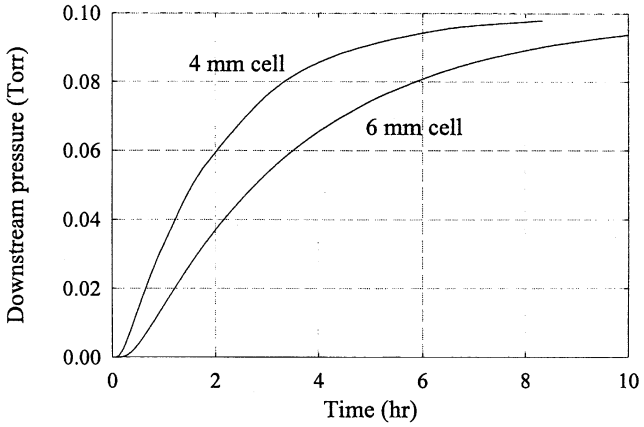

Figure 3. Effect of cell length on pressure response for *n*-butane.

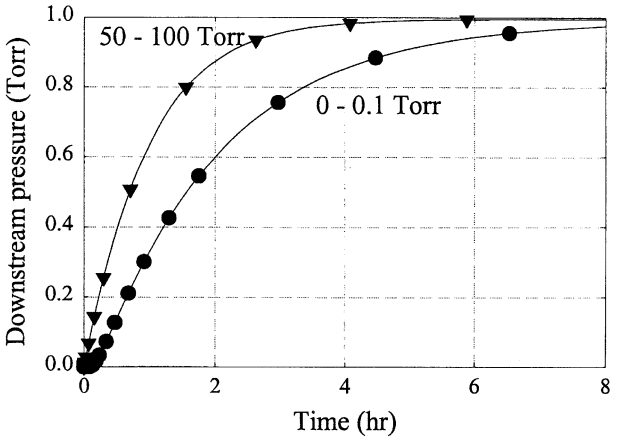

Figure 5. Effect of pressure step on pressure response for *n*-butane.

Effect of Pore Size. The effect of pore size is shown in Figure 4, where we see that the mass-transfer resistance is greater for smaller pores, as the Knudsen diffusion rate is proportional to r^3 and the viscous flow rate is proportional to r^4.

Effect of Loading. The effect of the difference in the initial pressure difference is shown in Figure 5. Two cases are dealt with here. In one case, the initial downstream pressure is 0 torr, while the upstream pressure is 0.1 torr. In the other case, however, the corresponding pressures are 50 and 100 torr, respectively. The pressure response shown in the figure has been normalized, and we note that the higher driving force in the latter case, as well as the smaller amount adsorbed between 50 and 100 torr compared to 0–0.1 torr (because of the convex isotherm), makes the kinetics much faster. Sigmoidal shape is observed in the case of 0–0.1 torr, while it is much less pronounced in the case of 50–100 torr.

Effect of Temperature. The effect of operation temperature is shown in Figure 6, where we see that the kinetics is faster with higher temperature. This is due to the smaller amount adsorbed at high temperature and the higher pore and surface diffusivities.

Intraparticle Temperature Profile. If the operation is carried out differentially, that is, the initial pressure difference between the two reservoirs is very small, the particle temperature change in most cases is less than 0.2°C. The effect of heat release is only important when the initial pressure difference is very large. We show this in the case where the initial pressure of the particle and the downstream reservoir is 0 and that of the upstream reservoir is 100 torr. Figure 7 shows the temperature profiles within the particle. We see that the temperature response exhibits a wavefront-type response. This temperature response corresponds to the pressure profile along the particle, as shown in Figure 8. The number on the temperature response curve corresponds to the pressure response curve of the same number.

We now show the potential of this mathematical model and the differential permeation technique by applying them to experimental data of propane, *n*-butane, and *n*-hexane to activated carbon.

Testing with experimental data of propane, n-butane and n-hexane

To test the potential of this method and the mathematical model presented in the second section, we validate the model

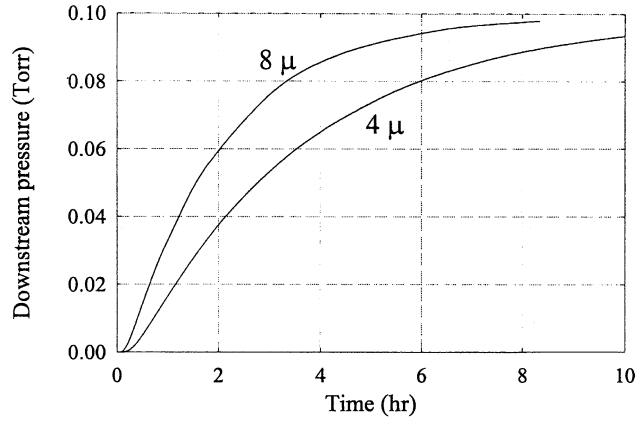

Figure 4. Effect of pore size on pressure response for *n*-butane.

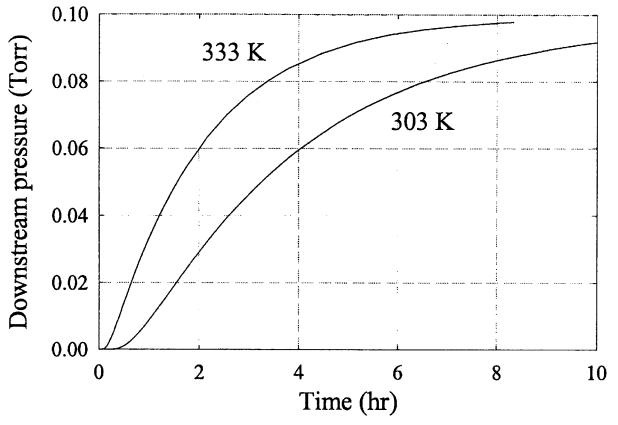

Figure 6. Effect of temperature on pressure response for *n*-butane.

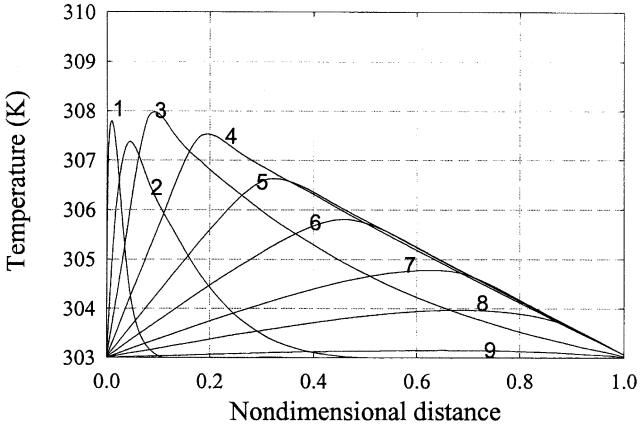

Figure 7. Typical temperature response for *n*-butane at 303 K.

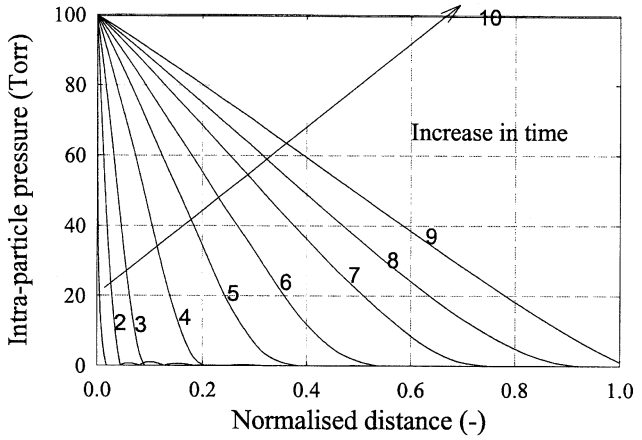

Figure 8. Typical intraparticle pressure profile for *n*-butane at 303 K.

against the permeation kinetics of propane, *n*-butane and *n*-hexane on an Ajax activated carbon, whose properties are given in Table 3.

The permeation experiments were conducted in a differential manner where the upstream and downstream pressures are kept close to each other. Before discussing the permeation data of propane, *n*-butane, and *n*-hexane, we first discuss the adsorption isotherm of these adsorbates collected at 303, 313, and 323 K for propane and *n*-butane, and at 313, 323, and 333 K for *n*-hexane.

Adsorption Isotherm. Analysis of the permeability data requires the accurate measurement of the adsorption isotherm.

Table 3. Properties of Activated Carbon

Particle density	0.733 g/cm^3
Total porosity	0.71
Macropore porosity	0.31
Average mesopore diameter	8×10^{-7} m
Micropore volume	0.44 cm^3/g
BET surface area	1,200 m^2/g

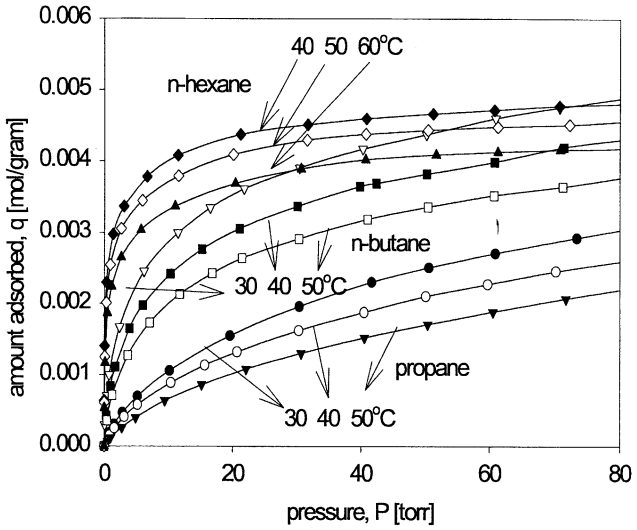

Figure 9. Adsorption isotherm of propane, *n*-butane, and *n*-hexane.

Isotherm data of propane, *n*-butane, and *n*-hexane were obtained with a high-accuracy volumetric apparatus. Isotherm data are shown as symbols in Figure 9. As seen, the adsorption affinity is on the order of *n*-hexane > *n*-butane > propane. The Langmuir equation cannot describe the isotherm data well due to the known strong heterogeneity of activated carbon.

Here we use the dual Langmuir equation for the description, and it was used to fit against the experimental data of all temperatures simultaneously (continuous lines in Figure 10).

$$C_\mu = C_{\mu s,1}\frac{b_1 P}{1+b_1 P} + C_{\mu s,2}\frac{b_2 P}{1+b_2 P}, \qquad (18a)$$

where

$$b_1 = b_{1,0}\exp\left[\frac{Q_1}{RT_0}\left(\frac{T_0}{T}-1\right)\right];$$

$$b_2 = b_{2,0}\exp\left[\frac{Q_2}{RT_0}\left(\frac{T_0}{T}-1\right)\right]. \qquad (18b)$$

Here T_0 is some reference temperature (taken as 303 K in this study), and $b_{1,0}$ and $b_{2,0}$ are the adsorption affinity constants at the reference temperature. The optimal parameters of the dual Langmuir isotherm derived from the fit between Eq. 18 and the data are given in Table 4.

Permeations Results. Using the adsorption isotherm information in the mathematical model, we match the simulated results against the permeation results expressed as the downstream pressure vs. time. The only fitting parameters for the permeation kinetics are the surface diffusivity at zero loading at the reference temperature, $D_{\mu 0}^{00}$, the activation energy for surface diffusion at zero loading, $E_{\mu 0}$, and the parameter β accounting for the decrease in the activation energy with

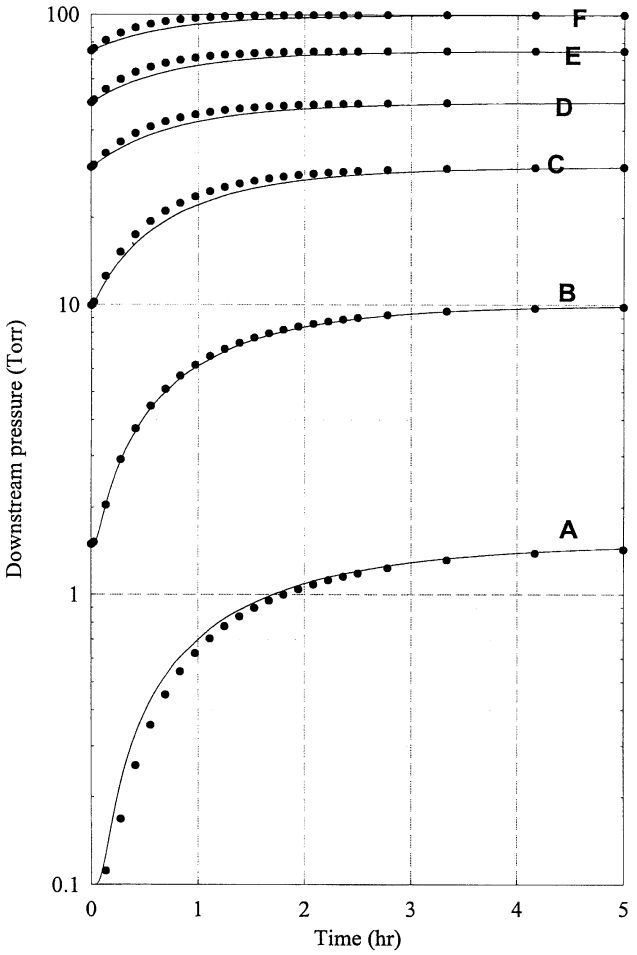

Figure 10. Downstream pressure vs. time for propane at 303 K.

loading. In all the figures to follow, the symbols represent experimental data and the solid lines are results from the mathematical model.

Propane Data. We first test the mathematical model with the transient permeation data of propane through activated carbon at 303 K. The data are presented as plots of downstream pressure vs. time, with the different level of pressure change as the parameter. This is shown in Figure 10 for 6 separate permeation runs. The labels on each curve correspond to the cases listed in Table 5 with the second column being the initial pressure for the particle and the downstream reservoir and the third column being the initial upstream reservoir. Since the upstream reservoir is very large in our experiment, the upstream pressure is almost constant during the whole course of the permeation run. The downstream reservoir pressure, however, will increase with time, and in general it exhibits a sigmoidal shape due to the initial penetration of the concentration wavefront through the particle. It eventually will increase to the same pressure as the upstream pressure. Take run *A*, for example, the initial pressure of the particle and the downstream reservoir is 0 torr, and the upstream reservoir pressure is maintained at 1.5 torr. When the permeation begins, the downstream pressure stays at almost 0 for about 5 min before it starts to increase; it eventually reaches 1.5 torr.

Table 4. Equilibrium Parameters for Propane, *n*-butane, and *n*-hexane

	Propane	*n*-Butane	*n*-Hexane
$C_{\mu s,1}$ (mol/m^3)	0.755×10^3	2.333×10^3	2.58×10^3
$C_{\mu s,2}$ (mol/m^3)	4.811×10^3	4.066×10^3	2.476×10^3
$b_{1,0}$ (1/Pa)	2.194×10^3	7.23×10^{-3}	0.331
$b_{2,0}$ (1/Pa)	1.02×10^{-4}	2.18×10^{-4}	4.15×10^{-3}
Q_1 (J/mol)	32,405	44,227	50,757
Q_2 (J/mol)	30,836	45,123	62,630

Table 5. Cases Corresponding to the Curves in Figure 10

	Init. Particle Pres. (torr)	Upstream Pres. (torr)
A	0.1	1.5
B	1.5	10
C	10	30
D	30	50
E	50	75
F	75	100

From fitting the mathematical model simultaneously against these six permeation runs at 303 K, we derive the following optimal parameters. The corrected surface diffusivity for propane at zero loading and at the reference temperature is 2.8×10^{-10} m^2/s. The value of β is 1.5×10^{-3}m ^{3}/mol, and the activation energy for surface diffusion is about 10,000 J/mol. When these parameters are used in the model to predict the permeation data at the other two temperatures (313 and 323 K), the results are in very good agreement with the experimental data. This supports the proposed mathematical model, which correctly accounts for various mass-transfer processes, as a tool to use in the description of permeation kinetics of hydrocarbon in activated carbon. The importance of surface diffusion among the three processes—pore diffusion, viscous flow, and surface diffusion—will be discussed later.

It is important to note here that the model was used to fit the many permeation data simultaneously and a good fit observed in all runs indicates the credibility of the model. Small difference is observed for permeation runs at high pressures. At those conditions, the adsorption loading in activated carbon is reasonably high, and therefore the mobility of the adsorbed molecules may not truly conform to the description of surface diffusion. It is likely that at high loadings adsorbed molecules form multilayers within the pore network and in some small pores liquid condensates are formed due to the high capillary forces. Therefore, hydrodynamics flow might become increasingly important, which is the reason why the model underpredicts the experimental data at high-pressure runs (see curves *C*, *D*, *E* and *F*).

n-Butane Data. As with the propane, the following figure (Figure 11) shows the permeation data of *n*-butane presented as plots of the downstream pressure vs. time at 303 K for seven different runs. Clearly, the mathematical model describes the system behavior very well, with the corrected surface diffusivity at zero loading, and at the reference temperature 303 K is 2×10^{-10} m^2/s. The value of β is 2.8×10^{-4} m^3/mol, and the activation energy for surface diffusion is

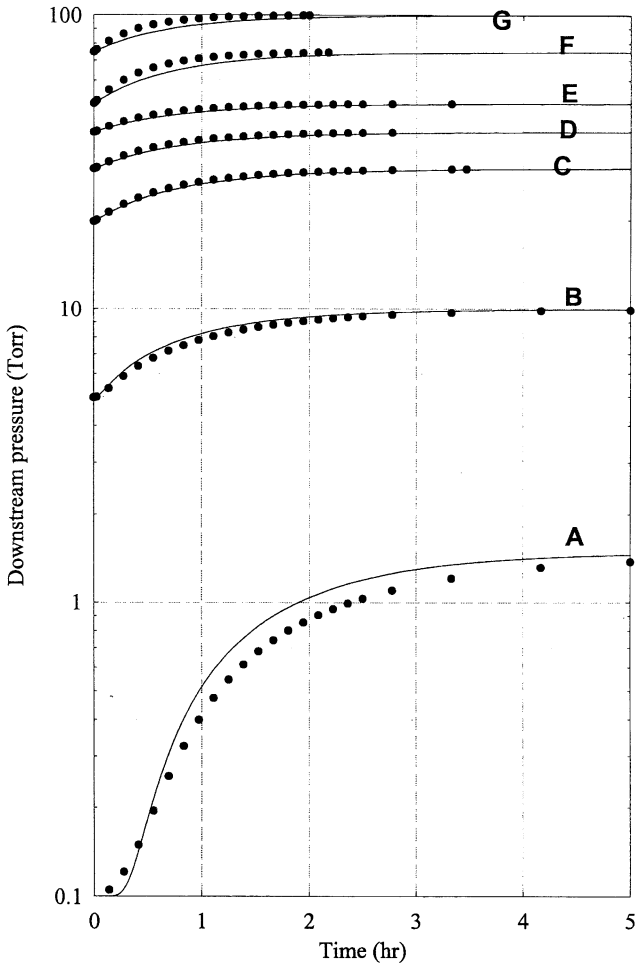

Figure 11. Downstream pressure vs. time for *n*-butane at 303 K.

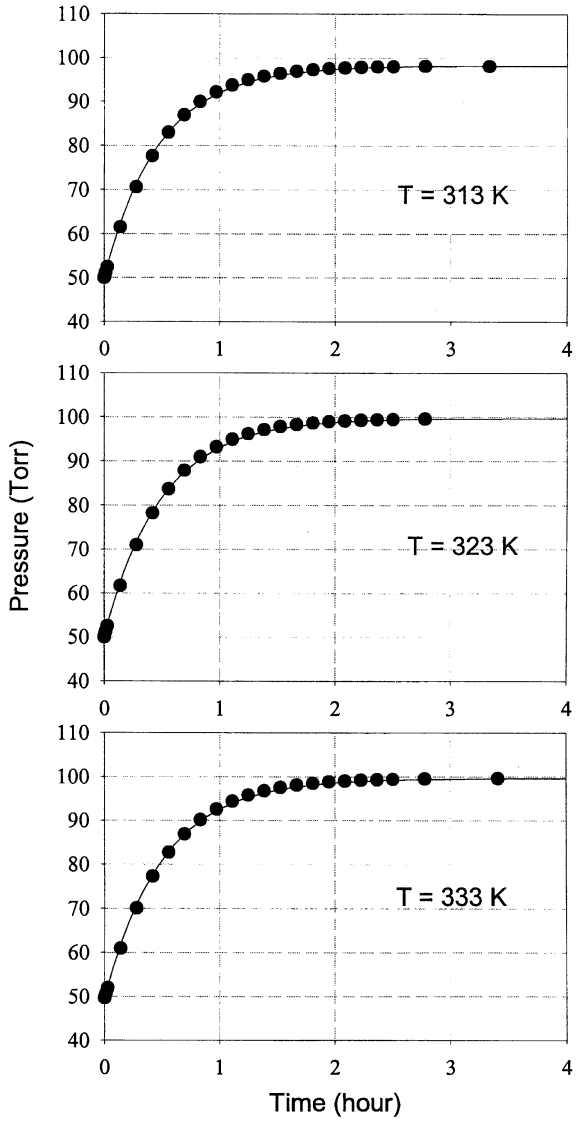

Figure 12. Downstream pressure vs. time for *n*-hexane at 313, 323 and 333 K.

about 15,000 J/mol. This same set of parameters (Table 6) is used to describe the permeation kinetics data at 313 and 323 K, and the predictions are very good in describing the data.

n-Hexane Permeation Data. The same conclusion can also be seen for *n*-hexane data at three temperatures 313, 323, and 333 K. The optimal parameters for the surface diffusivity at zero loading and at the reference temperature is 4.2×10^{-12} m^2/s, β of 4.2×10^{-14}, and $E_{\mu 0}$ of 25,000 J/mol. Figure 12 shows typical fitting between the model and the experimental data for *n*-hexane at 313, 323 and 333 K for the case where the initial pressure of the particle and the downstream reservoir is 50 Torr and the upstream pressure is maintained at 100 Torr. It is seen that the fit is very good. Comparing the surface diffusivity at zero loading and the activation energy for surface diffusion with those for propane and *n*-butane, we see that the surface diffusivity decreases with the carbon number, while the activation energy for surface diffusion increases with the carbon number. This is summarized in Table 7.

Knowing the heat of adsorption from the equilibrium study, we evaluate the ratio of the activation energy for surface dif-

Table 6. Cases Corresponding to the Curves in Figure 11

	Init. Particle Pres. (torr)	Upstream Pres. (torr)
A	0.1	1.5
B	5	10
C	20	30
D	30	40
E	40	50
F	50	75
G	75	100

Table 7. Surface Diffusion Parameters for Propane, *n*-Butane, and *n*-Hexane

	Propane	*n*-Butane	*n*-Hexane
$D_{\mu 0}^{00}$ (m^2/s)	2.8×10^{-10}	2.0×10^{-10}	4.23×10^{-12}
β (m^3/mol)	1.5×10^{-3}	2.8×10^{-4}	4.18×10^{-14}
$E_{\mu 0}$ (J/mol)	10,000	15,000	25,000

fusion to the heat of adsorption, and we find that this ratio increases from 0.35 of propane to 0.45 of *n*-hexane. The increase of this ratio with the carbon number is in agreement with the findings of Prasetyo and Do (1998, 1999), who used the constant molar flow method to determine the surface diffusivity.

Surface Diffusivity vs Loading. Having derived the surface diffusivity at zero loading, the activation energy for surface diffusion, we now investigate the behavior of the surface diffusivity vs. loading. The transport surface diffusivity is usually defined as

$$J_\mu = - D_\mu \frac{\partial C_\mu}{\partial r}. \tag{19}$$

Comparing this equation with Eq. 2c, used in our mathematical model, we see that the transport surface diffusivity is then given by

$$D_\mu = D_\mu^{00}(T) \exp\left(\frac{E_{\mu 0}}{RT}\frac{\beta C_\mu}{1+\beta C_\mu}\right)\frac{\partial \ln P}{\partial \ln C_\mu}, \tag{20}$$

where the first factor on the RHS of Eq. 20 is the surface diffusivity at zero loading, the second factor accounts for the variation of the activation energy with loading, and the last factor is known as the thermodynamic correction factor. Both of these factors increase with loading, which results in a greater increase in the transport diffusion coefficient with loading.

Table 7 shows that for the surface diffusion parameters for propane, *n*-butane, and *n*-hexane the decrease of surface diffusivity from propane to *n*-butane is quite modest, while the decrease from *n*-butane to *n*-hexane is quite rapid (from 2×10^{-10} to 4.23×10^{-10} m^2/s). This rapid change is almost probably due to the larger size of *n*-hexane (5.9 A, compared to 4.7 A of *n*-butane). This larger size results in the slower diffusion of *n*-hexane molecules within the micropore units (for the activated carbon used in this work, the mean micropore size is 8.6 A), and perhaps in the difficulty of the *n*-hexane molecules in penetrating the graphitic units (of dimension about 100 A) within the activated carbon structure. This significant drop in surface diffusivity has been well observed in zeolitic materials, where the term "configurational diffusion" has been coined, due to the comparable size between the diffusing molecules and the pore size. A similar phenomenon is also observed here for activated carbon.

The values of the surface-diffusion loading parameter need some discussion. As with the value of the surface diffusivity, the variation in the surface-diffusion loading parameter, β, between propane and *n*-butane is quite modest, while the value for *n*-hexane is much smaller. The small value of this latter parameter means that *n*-hexane can be described well by the Darken model (that is, no heterogeneity is reflected in the surface diffusion of *n*-hexane, meaning that to *n*-hexane molecules the surface seems to be relatively homogeneous), while smaller molecules such as propane and *n*-butane exhibit some degree of heterogeneity with respect to surface diffusion. While there is no clear justification (by experimental proof) for this, all we can conjecture for this observation is that the *n*-hexane molecule, being larger compared to propane and *n*-butane, can interact with various surface sites of varying energy simultaneously, and that therefore the energy barrier for *n*-hexane surface diffusion is an average of the energies of those sites. Propane and *n*-butane molecules, on the other hand, are smaller, and they therefore initially interact with stronger sites. As the loading increases, they adsorb onto sites of progressively lower energy with the result that the surface diffusion is relatively faster than what occurs initially.

Conclusion

This article has shown that the differential permeation method is a good tool for studying the surface diffusion of hydrocarbon gases and vapors in activated carbon. A number of observations were made from this study:

1. The dependence of the surface diffusivity on loading was found to be very strong, with its variation occurring over a few order of magnitude. The corrected surface diffusivity at zero loading decreases with an increase in molecular weight.
2. The permeation method, operated under differential conditions, is not affected by the heat effects, and the system can be run almost isothermally.

Acknowledgment

This project is supported by the Australian Research Council.

Literature Cited

Bulow, M., and A. Micke, "Determination of Transport Coefficients in Microporous Solids," *Adsorption*, **1**, 29 (1995).
Carman, P. C., *Flow of Gases through Porous Media*, Academic Press, New York, (1956).
Do, D. D., *Adsorption Analysis: Equilibria and Kinetics*, Imperial College Press, London (1998).
Do, D. D., "Dynamics of Adsorption in Heterogeneous Solids," *Equilibria and Dynamics of Gas Adsorption on Heterogeneous Solid Surfaces*, W. Rudzinski, W. Steele, and G. Zgrablich, eds., Elsevier, Amsterdam (1997).
Do, D. D., and K. Wang, "A New Kinetic Model for the Description of Adsorption Kinetics in Heterogeneous Activated Carbon," *Carbon*, **36**, 1539 (1998a).
Do, D. D. and K. Wang, "Dual Diffusion and Finite Mass Exchange Model for Adsorption Kinetics in Activated Carbon *AIChE J.*, **44**, 68 (1998b).
Johnson, M. F. L., and W. E. Stewart, "Pore Structure and Gaseous Diffusion in Solid Catalysts," *J. Catal.*, **4**, 248 (1965).
Kapoor, A., R. T. Yang, and C. Wong, "Surface Diffusion," *Catal. Rev. Sci. Eng.*, **31**, 129 (1989).
Nguyen, C., and D. D. Do, "A Dual Langmuir Kinetic Model for Adsorption in Carbon Molecular Sieve Materials," *Langmuir*, **16**, 1868 (2000).
Prasetyo, I., and D. D. Do, "Adsorption Rate of Methane and Carbon Dioxide on Activated Carbon by the Semi-Batch Constant Molar Flow Rate Method," *Chem. Eng. Sci.*, **53**, 3459 (1998).
Prasetyo, I., and D. D. Do, "Adsorption Kinetics of Light Paraffins in AC by a Constant Molar Flow Rate Method," *AIChE J.*, **45**, 1892 (1999).
Ruthven, D. M., "Principles of Adsorption and Adsorption Processes," Wiley, New York, (1984).
Sladek, K. J., E. R. Gilliland, and R. F. Baddour, "Diffusion on Surfaces. II. Correlation of Diffusivities of Physically and Chemically Adsorbed Species," *Ind. Eng. Chem. Fundam.*, **13**, 100 (1974).
Suzuki, M., *Adsorption Engineering*, Kodansha, Tokyo (1990).
Yang, R. T., *Gas Separation by Adsorption Processes*, Butterworth, New York, (1987).

Manuscript received Sept. 5, 2000, and revision received Apr. 9, 2001.